Polymer Journal (2020) 52:279–287
https://doi.org/10.1038/s41428-019-0284-2

ORIGINAL ARTICLE

X-ray scattering study on the changes in the morphology of low-modulus polypropylene under cyclic uniaxial elongation

Shotaro Nishitsuji[1] · Yuki Watanabe[2] · Tomoaki Takebe[3] · Nozomu Fujii[3] · Masaki Okano[3] · Mikihito Takenaka[4]

Received: 16 August 2019 / Revised: 9 October 2019 / Accepted: 9 October 2019 / Published online: 31 October 2019

Abstract

Low-modulus polypropylene (LMPP) with controlled stereoregularity was prepared based on the original catalyst technology [Minami et al. (Polym J 47:227–34, 2015)]. The LMPP showed elastic recovery, while plastic deformation was dominant in isotactic polypropylene. To understand the underlying mechanism, changes in the morphology of LMPP under cyclic uniaxial elongation were investigated using in situ small-angle X-ray scattering (SAXS) and wide-angle X-ray diffraction (WAXD). During the first cycle, yielding appeared in the stress–strain (S–S) curve, and the residual strain was large. The SAXS pattern is a ring pattern at strain zero and then changes to a four-point pattern and a two-point pattern with increasing strain. This four-point pattern is derived from the undulating structure of the crystal lamellae. During the stretching process, this undulation is large, and fragmentation of the lamellae occurs. Therefore, the residual strain increases. During the second cycle, no yield appeared in the S–S curve, and the residual strain was small. The SAXS pattern changed quickly from a four-point pattern to a two-point pattern. This result suggests that little fragmentation of the lamellae occurs and that only the lamellae were rotating under elongation. Thus, plastic deformation hardly occurs, and the residual strain decreases. Based on these results, lamella fragmentation has a significant effect on the elastic-recovery rate.

Introduction

Polypropylene (PP) is an excellent crystalline polymer with high ductility, good processability, and so on. It has already become an indispensable material in everyday life. Isotactic PP (iPP), which is presently in common use, is highly rigid due to its high degree of crystallinity. To further expand the use of iPP (for example, in nonwoven fabrics), it is necessary to have flexibility while maintaining a high ductility. The addition of a rubber component [1–5], copolymerization [6, 7], and so on represent suitable methods for giving iPP flexibility. However, since these methods are costly—due to the rubber and the molding process—it is desirable that iPP as a single component is flexible.

Controlling the stereoregularity of iPP is a convenient way to give the polymer more flexibility as a single component. Atactic PP (aPP), in which the directions of the methyl groups are completely disjointed, is an amorphous polymer, and its shape cannot be maintained at room temperature. Therefore, if it is possible to make an iPP material with a stereoregularity that is lower than that of regular iPP but higher than that of aPP, a new type of PP can be obtained that exhibits a lower melting point and crystallinity than that of regular iPP while maintaining its shape at room temperature and becoming softer. However, conventional catalysts cannot control the stereoregularity except for low molecular weight polymers [8].

De Rosa, Auriemma et al. synthesized new, low-stereoregularity iPP (LSiPP) materials using metallocene catalysts and investigated their tensile properties and

✉ Shotaro Nishitsuji
nishitsuji@yz.yamagata-u.ac.jp

[1] Department of Organic Materials Science, Graduate School of Organic Materials Science, Yamagata University, Yonezawa, Yamagata 992-8510, Japan

[2] Department of Polymer Chemistry, Graduate School of Engineering, Kyoto University, Nishikyo-ku, Kyoto 615-8510, Japan

[3] Performance Materials Laboratories, Idemitsu Kosan Co., Ltd., Ichihara, Chiba 299-0193, Japan

[4] Division of Multidisciplinary Chemistry, Institute for Chemical Research, Kyoto University, Uji 611-0011, Japan

morphology by wide-angle X-ray diffraction (WAXD) [9–12]. The authors succeeded in controlling the stereoregularity. Furthermore, in the stress–strain (S–S) curve, when the stereoregularity was lowered, yielding disappeared, similar to that with rubber. In other words, by controlling the stereoregularity, it was possible to obtain tensile properties between those of plastic and rubber. From the WAXD results, the authors found that the degree of crystallinity decreased with decreasing stereoregularity. In addition, they investigated the changes in the morphology of LSiPP by in situ small-angle X-ray scattering (SAXS) and WAXD [13, 14]. From the analysis of the WAXD patterns, they found that the LSiPP material has a disordered γ-form crystalline structure, which changes into an oriented mesomorphic form when stretched at room temperature and adopts an α-form crystalline structure when stretched at 60 °C. Analysis of the SAXS results showed that the LSiPP material exhibits a rod-like fibrillary morphology, including aggregates of mesomorphic crystals, when stretched at room temperature. On the other hand, at 60 °C, the morphology of LSiPP depends on the stereoregularity. If the stereoregularity is high, the LSiPP material consists of a fibrillary network, whereas if the stereoregularity is low, it is composed of rod-like fibrillary entities.

Recently, Idemitsu Kosan succeeded in developing a new low-modulus PP (LMPP) material with controlled stereoregularity based on the original catalyst technology [15]. The residual strain of LMPP is smaller than that of conventional PP when uniaxial elongation is repeatedly applied. This property demonstrates the elastic-recovery behavior of this material. While the mechanism behind this feature is still unclear, its elucidation is essential to further improve the performance of LMPP.

The purpose of this study is to clarify the mechanism of the elastic-recovery behavior of LMPP. To achieve this goal, the relationship between the morphology and the mechanical properties of LMPP is investigated because the morphology of crystalline polymers affects their mechanical properties. In particular, to investigate the elastic-recovery behavior, it is more effective to analyze the morphology under deformation. Therefore, in situ observations by SAXS and WAXD were performed under cyclic uniaxial elongation conditions; the stress was measured at the same time. To measure SAXS and WAXD under cyclic uniaxial elongation, a powerful X-ray source from a large synchrotron radiation facility is required. In recent years, changes in the morphology of iPP under elongation [16] and the morphology of iPP thin film on a substrate [17] have been actively studied. In this study, SAXS and WAXD measurements were performed under deformation by using a large synchrotron radiation facility, and changes in the morphology were observed.

Experimental procedure

Materials

The LMPP used in this study was provided by Idemitsu Kosan Co. Ltd (weight-average molecular weight: $M_w = 1.3 \times 10^5$, $M_w/M_n = 2.0$). Detailed information about LMPP can be found in reference [15]. After making a sheet by pressing the pellets at 230 °C, dumbbell specimens (JIS-K7113-2 1/2 size) were punched out.

DSC measurements

DSC was carried out under nitrogen flow at a heating and cooling rate of 10 K/min using Perkin-Elmer DSC-7. A tiny sample (~10 mg) for DSC was taken from the core part of a dumbbell specimen.

In situ SAXS/WAXD measurements

Simultaneous in situ SAXS/WAXD and stress measurements were performed while applying cyclic uniaxial elongation. The in situ SAXS and WAXD study was carried out at BL40B2 in SPring-8, Japan. The X-ray energy was 12.4 keV. For the SAXS experiments, the sample-to-detector distance was 1.25 m, and the scattering vector q range was 0.09–2 nm^{-1}, where q is the magnitude of the scattering vector defined by $q = \frac{4\pi}{\lambda}\sin\theta$, with λ and 2θ being the wavelength of the incident beam and the scattering angle in the medium, respectively. For the WAXD experiments, the sample-to-detector distance was 88.9 mm, and the q range was 5.5–22 nm^{-1}. All the scattering patterns were corrected for the sample transmittance and the scattering from the empty cell used in the experiments.

To impose cyclic uniaxial elongation, a hydraulic deformation tester was used. The details of the sample-deformation device are given elsewhere [18]. The strain rate was 1.0/min, and the maximum strain was 1.0. The time interval was 5.0 s, and the exposure time was 4.0 s, indicating that the data were obtained every 0.083 of strain. The detecting plane was set to the O_{xz} plane, where the O_x axis was the elongation direction and the O_z axis was the direction perpendicular to the elongation. The X-ray was introduced along the perpendicular direction O_y to the O_{xz} plane.

Results and discussion

As shown later in Figs. 4 and 6, the two-dimensional (2D) SAXS and WAXD patterns of LMPP before deformation are isotropic. We thus circularly averaged the 2D SAXS and WAXD patterns to analyze the morphologies quantitatively,

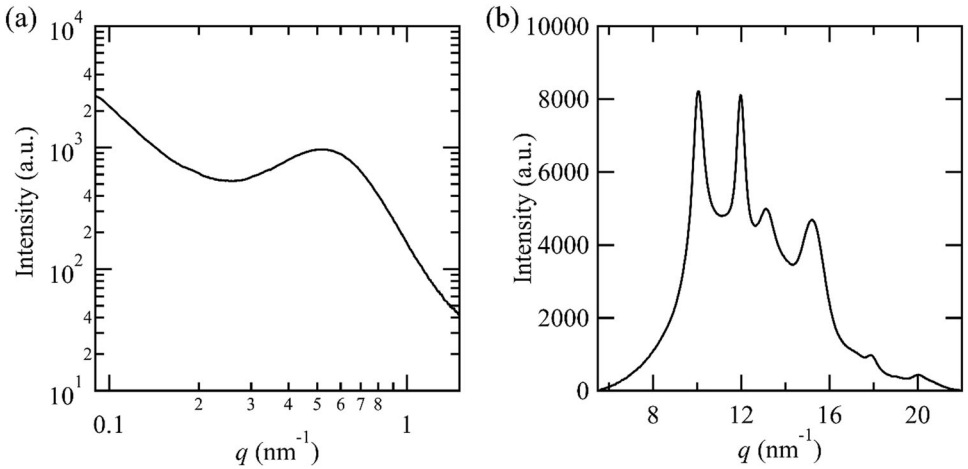

Fig. 1 The circular averaged scattering intensity is plotted as a function of q before cyclic uniaxial elongation: **a** SAXS and **b** WAXD

as shown in Fig. 1. There is a broad peak originating from the periodicity of lamellae in the SAXS profile. The long spacing of lamellae d_{ac} is estimated to be 9.7 nm from the peak position. We observed four diffractions (110), (040), (130), and (111) of the α crystal at 10.0, 11.9, 13.1, and 15.2 nm^{-1}, respectively, and a broad amorphous peak at 12.4 nm^{-1}. The peak separation in the scattering profile indicates that the degree of crystallinity is 18.8%, as estimated from the area.

Figure 2 shows the DSC curves of LMPP during the heating process and cooling process. Two peaks appear at 48.1 °C and 75.8 °C during the 1st heating in the DSC curve. However, 2nd heating shows a peak only at 78 °C. The peak at 48 °C in the 1st run originates from nonequilibrium crystals. Thus, the melting point is 75.8 °C. The degree of crystallinity is 16.1%, as estimated from the peak area of the DSC curve, and agrees with the WAXD result.

The S–S curve obtained for LMPP during the X-ray measurements is shown in Fig. 3. During the first cycle, the maximum stress is reached at 0.20 strain; then, yielding occurs, and the strain reaches a maximum value while the stress remains constant. Next, as the strain is reduced, the stress decreases monotonically, reaching a value of zero at 0.42 strain. This result means that LMPP does not recover its initial length and that a residual strain remains. During the second cycle, the stress starts to increase from 0.28 strain because the residual strain of the first cycle remains. The stress increases monotonically—without yielding—to the maximum strain. When the strain is reduced, the stress decreases monotonically and reaches a value of zero at 0.44 strain. Thus, the behavior of the stress differs greatly between the first and second cycles. The behavior after the third period is almost the same as that observed during the second period. The Young's modulus in the 1st cycle is 90.0 MPa, but in the 2nd cycle, it decreases to 8.17 MPa. Moreover, it becomes 8.13 MPa in the 3rd cycle, and there is almost no change from the 2nd

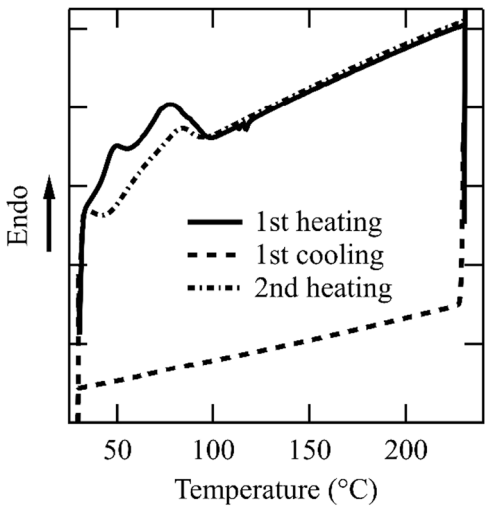

Fig. 2 DSC curves of LMPP during the heating process and cooling process

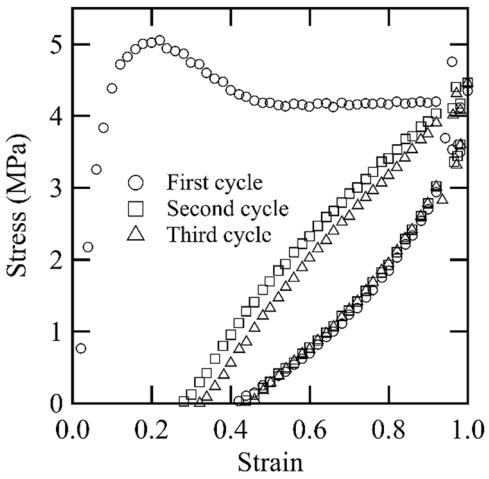

Fig. 3 The stress–strain curve of LMPP during an X-ray measurement

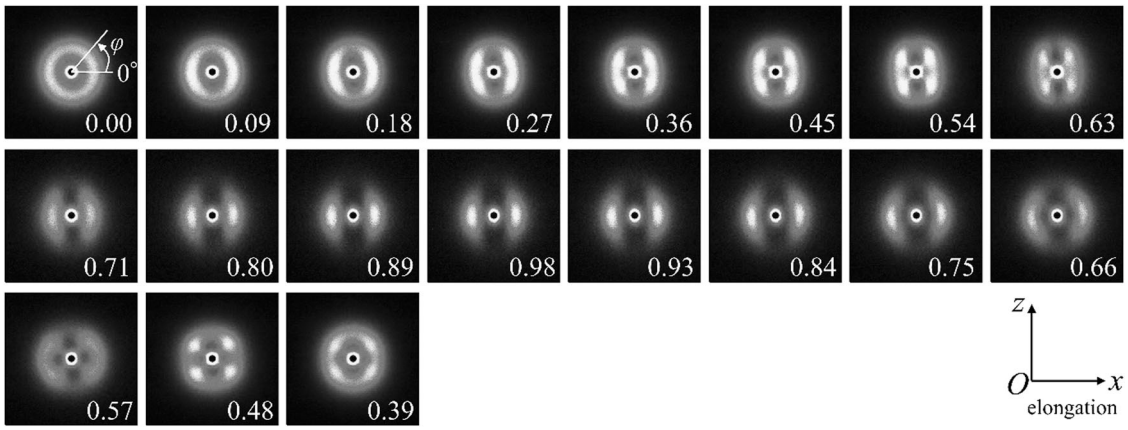

Fig. 4 Changes in the SAXS patterns under cyclic uniaxial elongation during the first cycle

cycle. Here, the elastic-recovery rate $R\%$ is defined by:

$$R = (1.0 - X) \times 100, \quad (1)$$

where X is the strain at which the stress starts to increase in the second cycle. As mentioned above, X is 0.28 strain. Therefore, R is estimated to be 72%. To clarify the mechanism of this elastic-recovery rate, the changes in morphology between the first and second cycles, where the stress behavior is largely different, are investigated.

Figure 4 shows the changes in the SAXS patterns of LMPP under cyclic uniaxial elongation during the first cycle. The number on the lower right of the figure indicates the strain. At strain zero, a ring-shaped scattering pattern appears. This correlation peak reflects d_{ac}. During the elongation process, the ring-shaped scattering pattern changes into a four-point pattern immediately after applying the strain. With the application of strain, a four-point pattern appears clearly, even at the 0.20 strain, which is the yielding point of the S–S curve. When the stress becomes constant, that is, when the strain exceeds 0.71, the scattering pattern changes into a two-point pattern. As the strain is reduced, the scattering pattern turns into a four-point image again and then adopts an almost ring-like scattering pattern. The strain in the ring-like scattering pattern is 0.39, which is the strain at which the stress is zero.

Figure 5a shows the scattering intensity as a function of the azimuthal angle φ at the peak position of the SAXS patterns. As shown in Fig. 4, it is defined that φ is zero at 3 o'clock and increases counterclockwise. The azimuthal profiles have four peaks immediately after applying the strain. As the strain increases, there are two peaks. When the strain is reduced, the azimuthal profiles have four peaks, and if there is no force, the azimuthal profiles do not show an azimuth dependency. The azimuthal angle of the peak in the first quadrant, φ_{peak}, was calculated from the SAXS patterns and plotted as a function of the elongation, as shown in Fig. 5b. As the strain increases, φ_{peak} increases when the scattering pattern is a four-point pattern. When the strain exceeds 0.71, φ_{peak} reaches a value close to zero, indicating that two peaks appear in the direction of the uniaxial elongation. When the strain is reduced, φ_{peak} is ~0.40. This value is much smaller than that measured during the elongation process.

When cyclic uniaxial elongation is applied to LMPP, the SAXS pattern adopts a four-point pattern. It has been reported that this four-point pattern also appears in the case of iPP [19–24]. According to the literature, this type of pattern derives from chevron structures. A compressive force applied in the direction perpendicular to the uniaxial elongation direction is responsible for this effect. This compressive force causes undulating structures in the crystal lamellae, and therefore, four-point patterns appear in the SAXS experiments. This undulating structure is called a chevron structure. In the case of LMPP, the undulating structures appeared immediately after applying the strain. As the strain increased, φ_{peak} increased as well, as shown in Fig. 5b, which indicates that undulation became stronger upon applying a compressive force. When the strain was increased further, fragmentation of the lamellae occurred at a certain strain, and the lamellae were drastically oriented in the direction of the uniaxial elongation. Therefore, the SAXS patterns changed into two-point patterns. As the strain was reduced, the scattering pattern changed again into a four-point pattern. However, φ_{peak} was small compared with the value determined during the elongation process, as mentioned above. Fragmentation of the lamellae occurred once during the elongation process, so it is thought that the lamellae do not experience much force and are only rotating. When the strain is ~0.42—a value at which the stress becomes zero—the SAXS patterns are almost isotropic. However, since lamella fragmentation has already occurred, the original lamella structure cannot be restored.

To estimate d_{ac} quantitatively, one-dimensional scattering profiles are calculated in the direction of the peak obtained with the azimuthal profiles. As shown in Fig. 5c,

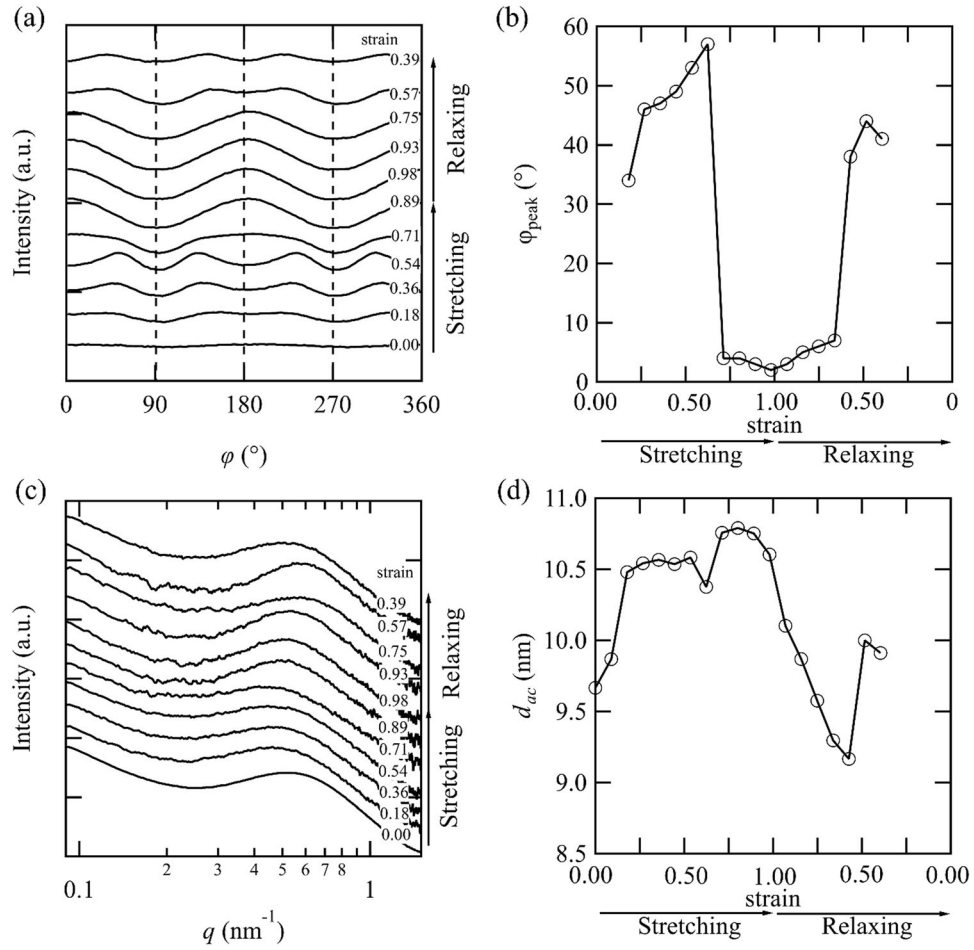

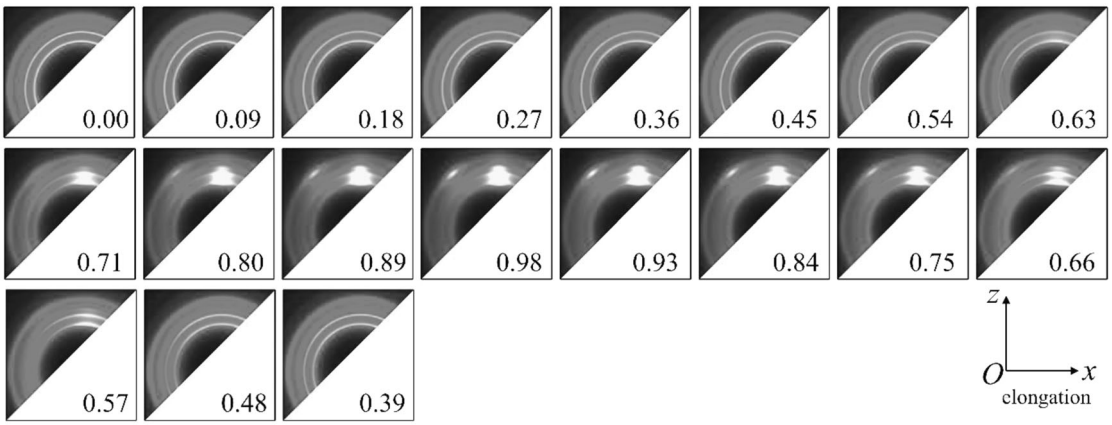

Fig. 5 **a** The azimuthal profiles at each strain under cyclic uniaxial elongation during the first cycle. The azimuthal angle zero is 3 o'clock from the center, and it increases counterclockwise. The strain changes from the bottom. **b** φ_{peak} is plotted as a function of the elongation during the first cycle. **c** Scattering profiles in the direction of the peak obtained with the azimuthal profiles during the first cycle. **d** d_{ac} values, estimated from the peak positions of the scattering profiles, plotted as a function of the strain during the first cycle

Fig. 6 Changes in the WAXD patterns under cyclic uniaxial elongation during the first cycle

the scattering profiles exhibit a broad peak reflecting d_{ac}. The value is estimated from the peak position of the scattering profiles, and the result is shown in Fig. 5d. The value of d_{ac} increases with increasing strain and decreases when the strain is reduced, reaching values lower than those observed before elongation. When the stress is zero (at ~40% strain), d_{ac} returns to its original value.

Figure 6 shows the changes observed in the WAXD patterns under cyclic uniaxial elongation during the first cycle. At strain zero, an isotropic scattering pattern appears, and there are four peaks reflecting (110), (040), (130), and (111). When the strain is increased, the scattering pattern adopts an isotropic form and does not change much. At 0.71 strain, diffractions corresponding to (110), (040), and

(130) appear on the meridian; these diffractions become sharp as the strain increases, indicating that the polymer chains are oriented along the direction of elongation. As the strain decreases, the anisotropy of the scattering patterns decreases, resulting in isotropic scattering patterns.

Next, the changes in the morphology during the second cycle were examined. Figure 7 shows the changes in the SAXS patterns under cyclic uniaxial elongation during the second cycle. The SAXS patterns are isotropic until stress is applied. They change into four-point patterns upon stress at a strain of 0.32 or more. As the strain increases, the pattern changes from a four-point to a two-point pattern. It can be seen that the strain changes to a two-point pattern with a small strain compared with the first cycle. Since the crystal lamellae have been fragmented once, they can be easily rotated. When the strain decreases, the SAXS pattern turns into a four-point pattern again, and when the stress is zero (at ~0.40 strain), it becomes isotropic. Similarly, as shown in Fig. 8a, when the strain increases, the SAXS pattern changes from a four-point to a two-point pattern, and when the strain is unloaded, it turns into a four-point pattern, which is isotropic. In addition, as shown in Fig. 8b, the

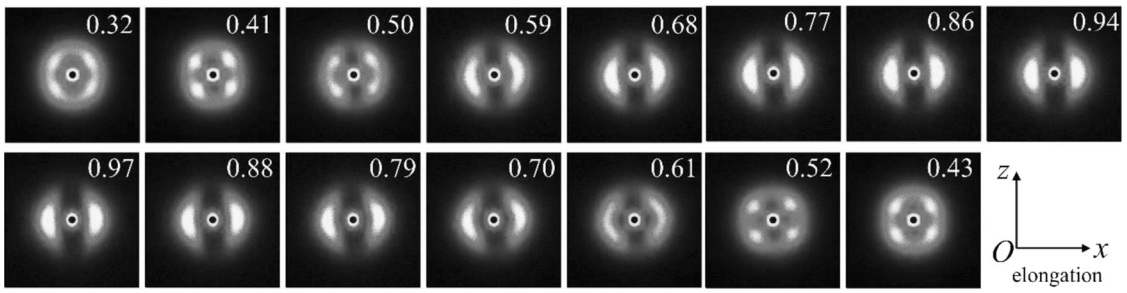

Fig. 7 Changes in the SAXS patterns under cyclic uniaxial elongation during the second cycle

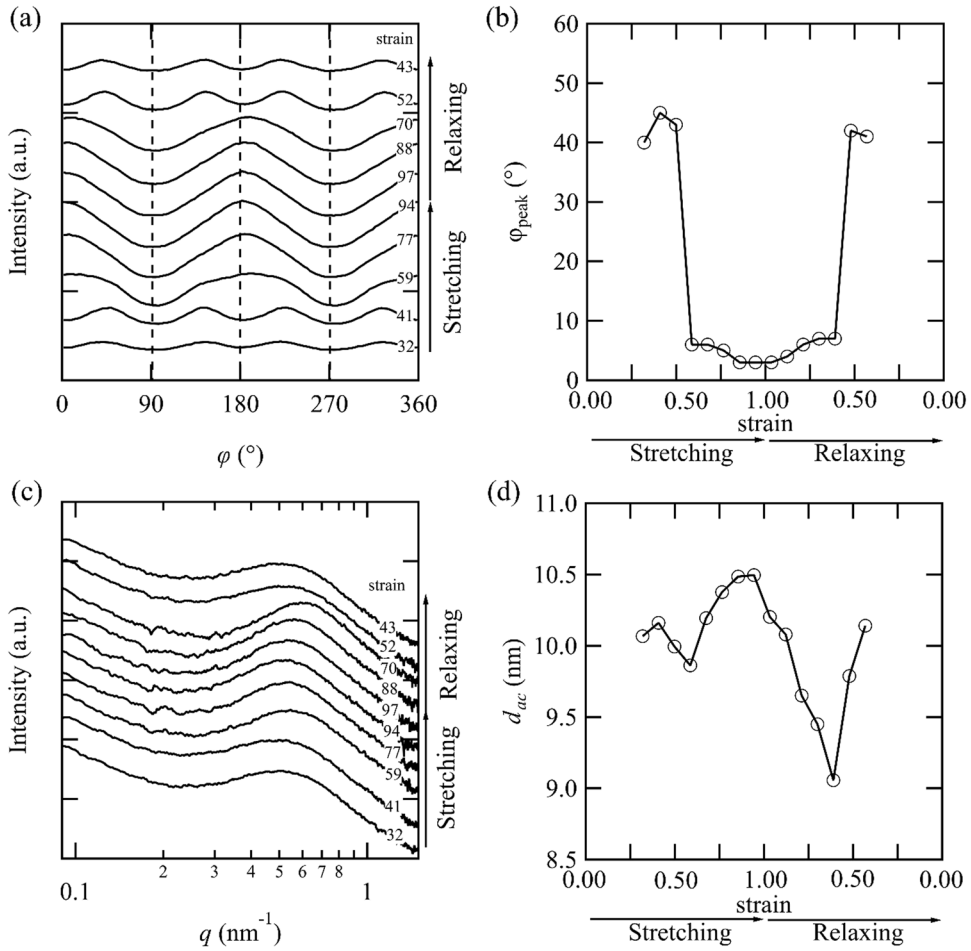

Fig. 8 **a** The azimuthal profiles at each strain under cyclic uniaxial elongation during the second cycle. **b** φ_{peak} is plotted as a function of the elongation during the first cycle. **c** Scattering profiles in the direction of the peak obtained with the azimuthal profiles during the second cycle. **d** d_{ac} values, estimated from the peak positions of the scattering profiles, plotted as a function of the strain during the second cycle

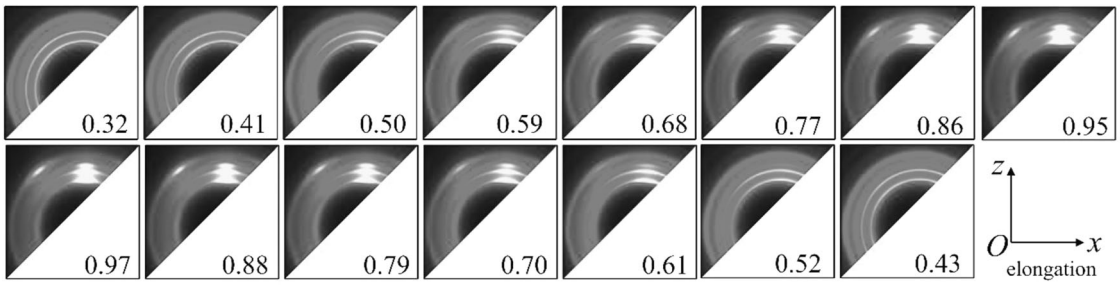

Fig. 9 Changes in the WAXD patterns under cyclic uniaxial elongation during the second cycle

value of φ_{peak} during the second cycle is smaller than that measured during the first cycle. This result occurs because lamella fragmentation occurs during the first cycle, so it is thought that the lamellae only rotate during the second cycle. Therefore, the four-point pattern immediately becomes a two-point pattern, and the lamellae are oriented with a small strain.

As shown in Fig. 8c, the scattering profile exhibits a broad peak—both in the first and second cycles—which corresponds to d_{ac}. d_{ac} increases with the strain and decreases when the strain is reduced, reaching a value smaller than that observed before elongation (similar to what happens during the first cycle). When the stress becomes zero (at ~0.40 strain), d_{ac} returns to its original value.

Figure 9 shows the changes observed in the WAXD patterns under cyclic uniaxial elongation during the second cycle. When the strain is increased, the scattering pattern adopts an isotropic form and does not change much. At 0.71 strain, diffractions corresponding to (110), (040), and (130) appear on the meridian; these diffractions become sharp as the strain increases, indicating that the polymer chains are oriented along the direction of elongation. As the strain decreases, the anisotropy of the scattering patterns decreases, resulting in isotropic scattering patterns.

The main difference between the first and second cycles is the fragmentation of the lamellae. Lamella fragmentation occurs during the first cycle, so the yield appears on the S–S curve. Since lamella fragmentation is a plastic deformation, the original structure cannot be restored. Fragmentation is directly related to the magnitude of the residual strain, which is especially large during the first cycle. On the other hand, during the second cycle, the lamellae only rotate, so no yield appears in the S–S curve and almost no plastic deformation, such as lamella fragmentation, occurs. Therefore, the residual strain during the second cycle is reduced. In addition, fragmented lamellae behave like physical cross-linking points and are considered to exhibit a rubber-like S–S curve during the second cycle.

In the case of general iPP, significant lamella fragmentation occurs, and voids are formed under elongation. As

Fig. 10 Photograph of LMPP under 1.00 strain

described above, lamella fragmentation is a plastic deformation that increases the residual strain. Furthermore, when a void is formed, the material will not readopt its original structure, which drastically increases the residual strain. Compared with that of general iPP, the degree of crystallinity of LMPP is small. Therefore, in both cases, fragmentation of the lamellae occurs, but the number of lamellae is greatly different, so that the residual strain is greatly affected. In the case of LMPP, since the number of crystal lamellae is small, the degree of lamella fragmentation, and therefore the amount of plastic deformation, should be small. In addition, in the case of LMPP, whitening does not occur at 1.00 strain, as shown in Fig. 10. This means that no voids are formed in LMPP. In other words, in the case of LMPP, only fragmentation of the lamellae affects the residual strain. This is the reason why the residual strain of LMPP is reduced in comparison with that of iPP.

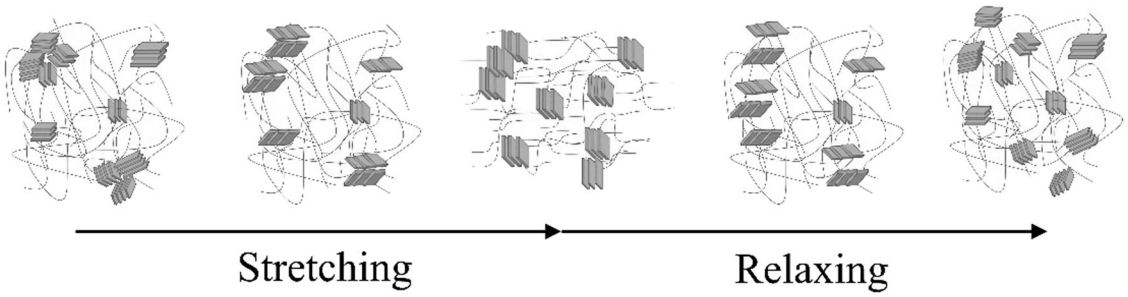

Fig. 11 A schematic diagram of the summary of changes in the morphology of LMPP

Conclusions

The changes in the morphology of LMPP under cyclic uniaxial elongation were investigated by in situ SAXS and WAXD. During the first cycle, yielding appeared in the S–S curve, and the residual strain was large. Upon elongation, the SAXS pattern changed from a ring pattern to a four-point pattern, and upon further elongation, it turned into a two-point pattern. When the strain decreased, the SAXS pattern changed into a four-point pattern again, and when the stress was zero, it adopted a ring pattern. This four-point pattern was derived from the undulating structure of the crystal lamellae, and the φ_{peak} value corresponding to the stretching process was found to be larger than that determined for the relaxation process. The value of d_{ac} increased with increasing strain and decreased when the strain was reduced. Furthermore, the WAXD pattern became strongly oriented in the case of a two-point SAXS pattern. These results indicate that no voids can be formed upon elongation but that lamella fragmentation (i.e., plastic deformation) occurs and the residual strain increases. During the second cycle, no yield appeared in the S–S curve, and the residual strain was small. The SAXS pattern quickly changed from a four-point to a two-point pattern, and the φ_{peak} corresponding to the stretching and relaxation processes had the same value as that observed during the relaxation process of the first cycle. Our results indicate that little fragmentation of the lamellae occurred and that the lamellae were only rotated upon elongation. This observation means that plastic deformation hardly occurred, reducing the residual strain. Figure 11 shows a schematic diagram of the summary of changes in the morphology of LMPP. Based on these results, we propose that lamella fragmentation has a significant effect on the elastic-recovery rate. Moreover, if the degree of crystallinity of LMPP can be further reduced by controlling the stereoregularity, the amount of lamella fragmentation can be controlled, and the elastic-recovery rate of LMPP should be controllable.

Acknowledgements The synchrotron radiation experiments were performed at the BL40B2 of SPring-8 with the approval of the Japan Synchrotron Radiation Research Institute (JASRI) (Proposal No. 2016A1441).

Compliance with ethical standards

Conflict of interest The authors declare that they have no conflict of interest.

Publisher's note Springer Nature remains neutral with regard to jurisdictional claims in published maps and institutional affiliations.

References

1. Jang BZ, Uhlmann DR, Vandersande JB. The rubber particle-size dependence of crazing in polypropylene. Polym Eng Sci. 1985; 25:643–51.
2. Nomura T, Nishio T, Sato H, Sano H. Study of super olefin polymer by the control of nano-order structure. 1. Mechanical-properties and morphology of the polypropylene and ethylene propylene rubber blends. Kobunshi Ronbunshu. 1993;50:19–25.
3. Nitta K, Okamoto K, Yamaguchi M. Mechanical properties of binary blends of polypropylene with ethylene-alpha-olefin copolymer. Polymer. 1998;39:53–8.
4. Naiki M, Matsumura T, Matsuda M. Tensile elongation of high-fluid polypropylene/ethylene-propylene rubber blends: dependence on molecular weight of the components and propylene content of the rubber. J Appl Polym Sci. 2002;83:46–56.
5. Zhang B, Fu ZS, Fan ZQ, Phiriyawirut P, Charoenchaidet S. Preparation and characterization of high mfr polypropylene and polypropylene/poly(ethylene-co-propylene) in-reactor alloys. J Appl Polym Sci. 2016;133. https://doi.org/10.1002/app.42984.
6. Sun YY, Fu LL, Wu ZH, Men YF. Structural evolution of ethylene-octene copolymers upon stretching and unloading. Macromolecules. 2013;46:971–6.
7. Zhao JY, Sun YY, Men YF. Elasticity reinforcement in propylene-ethylene random copolymer stretched at elevated temperature in large deformation regime. Macromolecules. 2016;49: 609–15.
8. Mise T, Miya S, Yamazaki H. Excellent stereoregular isotactic polymerizations of propylene with c2-symmetric silylene-bridged metallocene catalysts. Chem Lett. 1989;18:1853–6.
9. De Rosa C, Auriemma F. Single site metallorganic polymerization catalysis as a method to probe the properties of polyolefins. Polym Chem. 2011;2:2155–68.
10. De Rosa C, Auriemma F, De Lucia G, Resconi L. From stiff plastic to elastic polypropylene: polymorphic transformations during plastic deformation of metallocene-made isotactic polypropylene. Polymer. 2005;46:9461–75.

11. De Rosa C, Auriemma F, Di Capua A, Resconi L, Guidotti S, Camurati I, Nifant'ev IE, Laishevtsev IP. Structure-property correlations in polypropylene from metallocene catalysts: stereodefective, regioregular isotactic polypropylene. J Am Chem Soc. 2004;126:17040–9.
12. De Rosa C, Auriemma F, Perretta C. Structure and properties of elastomeric polypropylene from c-2 and c-2v-symmetric zirconocenes. The origin of crystallinity and elastic properties in poorly isotactic polypropylene. Macromolecules. 2004;37:6843–55.
13. Auriemma F, De Rosa C, Di Girolamo R, Malafronte A, Scoti M, Mitchell GR, Esposito S. Deformation of stereoirregular isotactic polypropylene across length scales. Influence of Temperature. Macromolecules. 2017;50:2856–70.
14. Auriemma F, De Rosa C, Di Girolamo R, Malafronte A, Scoti M, Mitchell GR, Esposito S. Time-resolving study of stress-induced transformations of isotactic polypropylene through wide angle x-ray scattering measurements. Polymers. 2018;162:10.
15. Minami Y, Takebe T, Kanamaru M, Okamoto T. Development of low isotactic polyolefin. Polym J. 2015;47:227–34.
16. Kurihara H, Kitade S, Ichino K, Akiba I, Sakurai K. Elongation induced beta- to alpha-crystalline transformation and microvoid formation in isotactic polypropylene as revealed by time-resolved waxs/saxs. Polym J. 2019;51:199–209.
17. Uchida K, Mita K, Higaki Y, Kojio K, Takahara A. Lamellar orientation in isotactic polypropylene thin films: a complement study via grazing incidence x-ray diffraction and surface/cross-sectional imaging. Polym J. 2019;51:183–8.
18. Suehiro S, Saijo K, Ohta Y, Hashimoto T, Kawai H. Time-resolved detection of x-ray-scattering for studies of relaxation phenomena. Anal Chim Acta. 1986;189:41–56.
19. Li JX, Cheung WL, Chan CM. On deformation mechanisms of beta-polypropylene 3. Lamella structures after necking and cold drawing. Polymer. 1999;40:3641–56.
20. Krumova M, Henning S, Michler GH. Chevron morphology in deformed semicrystalline polymers. Philos Mag. 2006;86:1689–712.
21. Lezak E, Bartczak Z. Plastic deformation of the gamma phase isotactic polypropylene in plane-strain compression at elevated temperatures. Macromolecules. 2007;40:4933–41.
22. Lezak E, Bartczak Z, Galeski A. Plastic deformation behavior of beta-phase isotactic polypropylene in plane-strain compression at room temperature. Polymer. 2006;47:8562–74.
23. Lezak E, Bartczak Z, Galeski A. Plastic deformation of the gamma phase in isotactic polypropylene in plane-strain compression. Macromolecules. 2006;39:4811–9.
24. Chang BB, Schneider K, Xiang F, Vogel R, Roth S, Heinrich G. Critical strains for lamellae deformation and cavitation during uniaxial stretching of annealed isotactic polypropylene. Macromolecules. 2018;51:6276–90.